

**APPLICATION OF openFOAM IN NUMERICAL SIMULATIONS OF HIGH-SPEED
TRAINS AERODYNAMICS**

Panpan Lu

School of Engineering Science,
University of Chinese Academy of Sciences,
Beijing, 100049, China

Key Laboratory for Mechanics in
Fluid Solid Coupling Systems,
Institute of Mechanics,
Chinese Academy of Sciences,
Beijing, 100190, China
Email: lupanpan@imech.ac.cn

Guowei Yang

Key Laboratory for Mechanics in
Fluid Solid Coupling Systems
Institute of mechanics
Chinese academy of sciences
Beijing China
Email: gwyang@imech.ac.cn

Bo Yin*

Key Laboratory for Mechanics in
Fluid Solid Coupling Systems
Institute of mechanics
Chinese academy of sciences
Beijing China
Email: yinbo@imech.ac.cn

Zhanling Ji

Key Laboratory for Mechanics in
Fluid Solid Coupling Systems
Institute of mechanics
Chinese academy of sciences
Beijing China
Email: 149018663@qq.com

ABSTRACT

The present study uses openFOAM package to simulate and investigate the aerodynamic performance and characteristics of high-speed trains (velocity beyond 250 km/h) under typical and critical conditions, which include flow passing a high-speed train, and two trains meeting towards each other at the same velocity in the open air. In terms of different operation conditions, separate openFOAM solvers are adopted. For flow passing a high-speed train at a constant velocity, a steady solver for incompressible, viscous and turbulent flow is employed on a fixed mesh and the results are compared with commercial software Star CCM+. For trains meeting towards each other, overset mesh method is used in which inverse distance interpolation is taken to couple background and inner overset mesh. The built-in mesh generation tool SnappyHexMesh is utilized to generate background and inner overset mesh. In all simulations, $k-\omega$ SST two equations RANS model is used to simulate the turbulent flow.

Introduction

Aerodynamics is a sub-field of fluid dynamics, which studies the motion of air around an object exclusively. Obtaining the flow field enables the calculation of forces and moments acting upon the object. In the majority of aerodynamic problems, the quantities of interest include forces and moments. Flow around bluff bodies can be seen everywhere and play a significant role in our daily life, which is an important phenomenon in aerodynamics. The investigation of flow around high-speed trains is one of the most practical applications of bluff body studies. Compared with automobiles and airplanes, high-speed trains have the advantages of fast speed, large transportation volume, less land occupation and low energy consumption. With comprehensive advantages, high-speed trains will play an increasingly important role in the future world transportation system. Over the past few decades, many experimental simulations and investigations have been conducted by researchers. Aerodynamic forces and moments on scale model were investigated in wind tunnel [1]. Besides, the influence of Reynolds number on the aerodynam-

*Address all correspondence to this author.

ic drag forces were investigated experimentally [2]. Some researchers [3] studied the influence of train velocity and the nose shape on the flow structure. Some investigations [4–11] on side wind effect on aerodynamic performance and characteristics of high-speed train were performed. In recent years, Chinese high-speed trains designed by aerodynamic characteristics were developed and aerodynamic optimization was presented [12, 13]. The calculation of aerodynamic drag force of high-speed train passing a tunnel was conducted [14, 15]. The influence of turbulent intensity on the aerodynamic force and pressure coefficient of high-speed train was studied. [16]

Considering the high cost of experimental investigations, numerical simulation is an alternative method to obtaining the aerodynamic properties. Turbulent models used in numerical calculation of aerodynamic performance of high-speed train generally include RANS, LES, DES, which include the aerodynamic performance of high-speed trains under side wind [17–20], the alteration in aerodynamic forces when high-speed train entering a tunnel [21–24], the aerodynamic optimization of high-speed trains by reducing drag force to decrease energy consumption [25–27], the impact of moving ground and rotating wheels on the aerodynamic drag and wake flow structure behind the high-speed train [28]. Numerical simulations mentioned above were performed with commercial CFD software such as Fluent, Star CD, Star CCM+. openFOAM is an object-oriented library for Computational Continuum Mechanics, which in the paper, numerical simulations about high-speed trains are performed by Openfoam from the mesh generation, discretization to field variables solution.

Numerical Method Mesh Generation

The main purpose of the paper is to discuss the numerical simulations by openFOAM. Therefore, the high-speed train model is simplified and shown in the Figure 1. The procedure to generate mesh by snappyHexMesh is introduced and then the critical parameters for adding boundary layers are given. Background mesh must be created before snappyHexMesh is executed, which is comprised of hexahedral cells filling the entire region. The process of generating a mesh using snappyHexMesh is controlled by three steps. In the first step, cell splitting at feature edges and surface is performed according to the castellatedMeshControls sub-dictionary specified by user. After cell splitting is finished, cells whose volume are less than 50% are removed within the region in which cells are retained. In the second step, vertices in the castellated boundary are moved to the geometry surface, and then the internal mesh is resolved with the latest displaced boundary vertices. If there are vertices leading to mesh quality parameters to be violated, the displacement will be reduced and repeat the processes mentioned above until mesh quality is satisfied. In the last step, mesh layer addition is conducted to create boundary layer in which the mesh is projected back from the surface by a specified thickness in the direction normal to the surface. In all cases, the first boundary layer thickness, expansion ratio and the total number of boundary layer is set to 0.001m, 1.2 and 8 respectively. The volume mesh configuration and boundary layer setup is shown in the Figure 2.

uration and boundary layer setup is shown in the Figure 2.

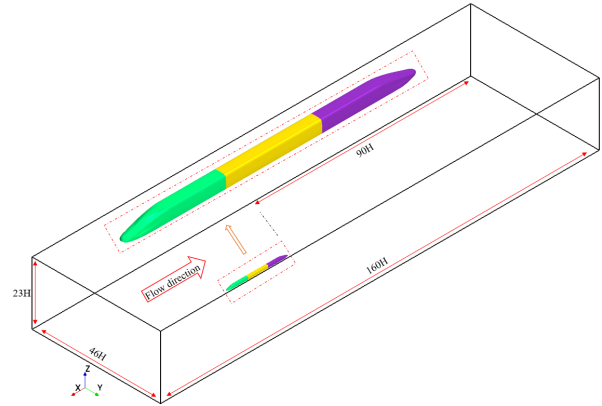


FIGURE 1. Simplified CRH380A model and computational region

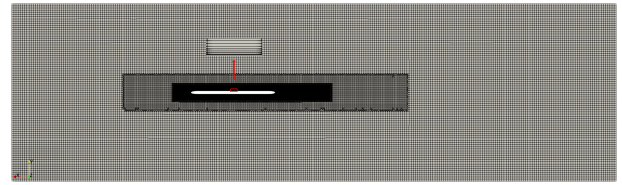


FIGURE 2. Volume mesh configuration and boundary layer

Governing Equations Discretization

In the subsection, the governing equations discretization in the fluid dynamics will be introduced. The general transport equation for the given transport quantity ϕ is solved in the given fluid field and with given boundary conditions and initial conditions. The general transport equation can be expressed as follows:

$$\int_{V_p} \frac{\partial \rho \phi}{\partial t} dV + \int_{V_p} \nabla \cdot (\rho \mathbf{u} \phi) dV - \int_{V_p} \nabla \cdot (\rho \Gamma_\phi \nabla \phi) dV = \int_{V_p} S_\phi(\phi) dV \quad (1)$$

Applying Gauss theorem to convert the volume integrals to surface integrals yields to the following discrete equations:

$$\int_{V_p} \frac{\partial \rho \phi}{\partial t} dV + \sum_f S_f \cdot (\rho \mathbf{u} \phi)_f - \sum_f S_f \cdot (\rho \Gamma_\phi \nabla \phi)_f = S_c V_p + S_p V_p \phi_p \quad (2)$$

Specially, for the source term, the approximation is at least second order accurate. S_c is the linear part of the source term and S_p is the non-linear part.

There are several built-in schemes in openFOAM to discretize terms, such as interpolation schemes referring to the method used to interpolate values from cell centers to face centers, surface normal gradient schemes referring to method used to evaluate the surface normal gradient at the faces. The information related to the discretization schemes for the different terms appearing in the governing equations is located at the fvSchemes dictionary.

Solver and Algorithm

The default solver supplied by openFOAM for the simulation of flow passing high-speed train is simpleFoam, It is a steady-state solver for incompressible, turbulent flow, which is based on SIMPLE [29] algorithm to solve the pressure-velocity coupling. The Semi-Implicit Method for Pressure-Linked Equations(SIMPLE) enables the calculation of pressure from velocity components by coupling the Navier-Stokes equations with iterative procedure. There are several methods offered by openFOAM to solve the set of linear equations. Before solving an equation of a particular field, the initial residual is evaluated based on the current values of the field. After each solver iteration, the residual is evaluated again based on the new values of the field. when one of control parameters including tolerance, reTol, and maxIter is reached, the solver stops. The detailed information on solvers and algorithm is in fvSolution dictionary.

Overset Mesh Technology

Overset Mesh technology is used for both static and dynamic cases. A composite computational domain is generated by employing cell-to-cell mapping between multiple disconnected mesh regions. This enables the simulation of complex mesh motions and interaction without penalties related to deforming meshes. Overset mesh technology is used to simulate the high-speed train passing a tunnel and two high-speed trains meeting. Focusing on the application of overset mesh, the practical running condition, high-speed train passing a tunnel or two high-speed trains meeting, is substituted for a high-speed train running in open air. The default solver supplied by openFOAM for the simulation of a high-speed train running in open air is overPimpleDyMFOam, It is a transient solver for incompressible, turbulent flow on a moving mesh, which is based on PIMPLE (merged PISO-SIMPLE) algorithm to solve the pressure-velocity coupling. In the fvSchemes dictionary, additional overset interpolation scheme is need to couple overlapping regions.

Results and Discussion

In the previous parts, the computational fluid dynamics procedures set up in openFOAM are introduced separately, which include mesh generation, discretization schemes, solver and algorithm. In order to compare the numerical simulation results of flow passing a high-speed train between Star CCM+ and openFOAM, the computational region sizes, mesh sizes, turbulence simulation methods are same. Both numerical simulations are conducted using RANS numerical method and $k-\omega$ SST turbulence model.

Comparison of Pressure Distribution

Figure 3 shows the pressure distribution around head train in the case of flow passing high-speed trains. The maximum pressure is reached at the nose tip of head train. Air passing either above or below the stagnation point increase its velocity magnitude and decrease the pressure forces acting on the high-speed trains surface. For both results from openFOAM and Star CCM+, the pressure distribution around the head train are

similar and corresponding to the analysis above. However, the pressure value are different from each other. Specifically, at the stagnation point, the pressure value about 4700Pa calculated by openFOAM is lower than the value about 7200Pa calculated by Star CCM+. Moreover, the overall pressure value by Star CCM+ is greater than that of openFOAM. Obviously, the difference in pressure values will lead to the discrepancy in drag coefficient of head train.

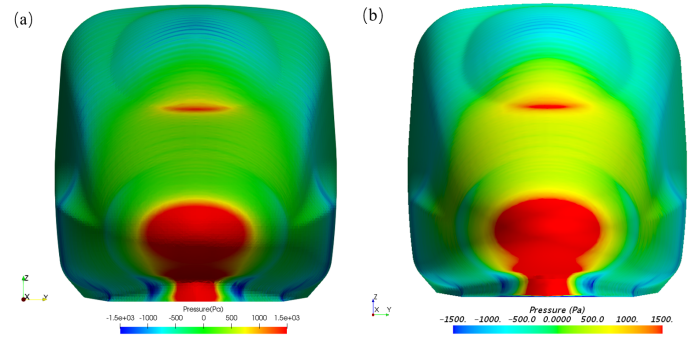


FIGURE 3. Comparison of pressure distribution around head train; (a) by openFOAM, (b) by Star CCM+

Due to the existence of back pressure gradient, flow separation occurs and leads to negative pressure area appearing around the streamline transition part of tail train. Additionally, there are a lot of vortices in the wake region causing pressure disturbance, which leads to positive pressure at the nose tip of tail train. It is found that the pressure distribution on the head train and tail train is similar, however, the pressure value of head train is generally larger than that of tail train. The main distinction of pressure distinction around tail train between openFOAM and Star CCM+ is that the magnitude of negative pressure around driver's cab by openFOAM is smaller than that by Star CCM+, but the positive pressure of tail nose tip by openFOAM is larger than that by Star CCM+.

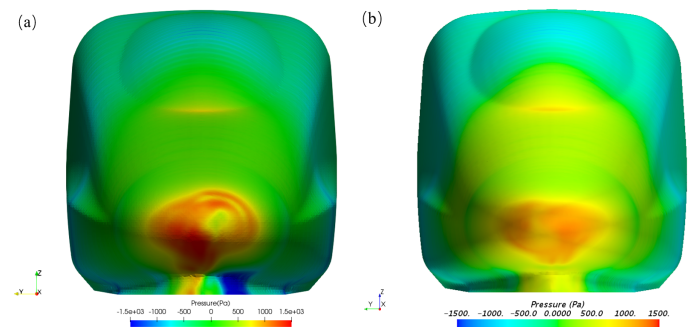


FIGURE 4. Comparison of pressure distribution around tail train; (a) by openFOAM, (b) by Star CCM+

Comparison of Velocity Distribution

Air stagnating in front of the nose tip of head train accelerates downstream and reaches the maximum velocity near driver's cab where surface curvature changes sharply. In addition, near driver's cab of tail train, air velocity reaches another local maximum, where flow separation occurs. Velocity distribution

obtained by openFOAM and Star CCM+ in the coronal section is similar with each other basically and conforms to above analysis. However, the velocity distribution by them at the bottom of trains varies largely. Specifically, velocity magnitude by Star CCM+ is generally larger than that of openFOAM at the same position, indicating that the energy dissipation of the latter is faster.

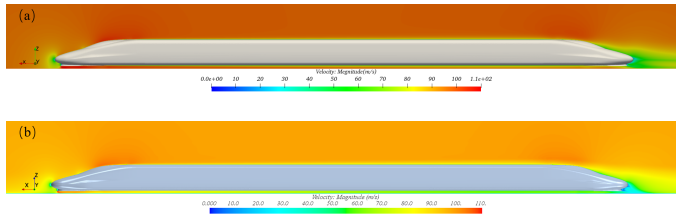


FIGURE 5. Comparison of velocity distribution; (a) by openFOAM, (b) by Star CCM+

Comparison of Drag Coefficient

The drag coefficient is defined as follows:

$$C_d = \frac{F_d}{\frac{1}{2}\rho u^2 S} \quad (3)$$

Where F_d stands for drag force; ρ is density of air; u and S stand for velocity and cross-sectional area of trains.

Table 1 shows the drag coefficient of three-group high-speed trains by openFOAM and Star CCM+. Obviously, the drag coefficient of head train by Star CCM+ is larger than that by openFOAM and the distinction of middle train is the smallest among the three carriages. Moreover, the drag of tail train varies dramatically and the drag by openFOAM is almost twice that by Star CCM+.

	head	middle	tail	total
openFOAM	0.0654	0.0465	0.057	0.1689
Star CCM+	0.0866	0.0411	0.028	0.1559

TABLE 1. Drag Coefficient by openFOAM and Star CCM+

Application of Overset Mesh Method

The cells with blue color are known as calculated cells in which the solution is computed. The cells with green color are interpolated cells in which the solution is interpolated from mesh to mesh. The red cells are called as hole in which solution is not computed. The details of volume cell types can be found in FIGURE 6.

Pressure distribution at different time in the case of two trains meeting towards each other is shown in FIGURE 7. At the time of 0.05s, the pressure distribution in the zone between two trains is basically the same as that of far field. When two trains are about to meet, the positive pressure of zone in front of head train increases significantly. After the head trains passing each other, there is a negative pressure zone in the overlapping area of the two trains. In general, as two trains get closer, the

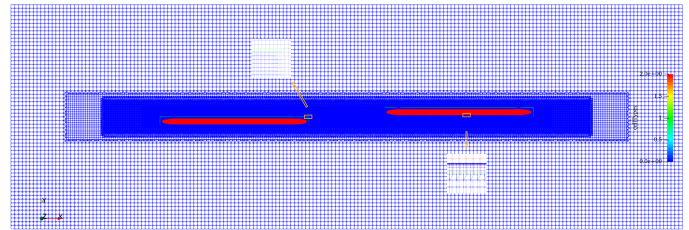


FIGURE 6. Cell types of coupled volume mesh interaction between them continues to become stronger and the aerodynamic force acting on trains changes gradually.

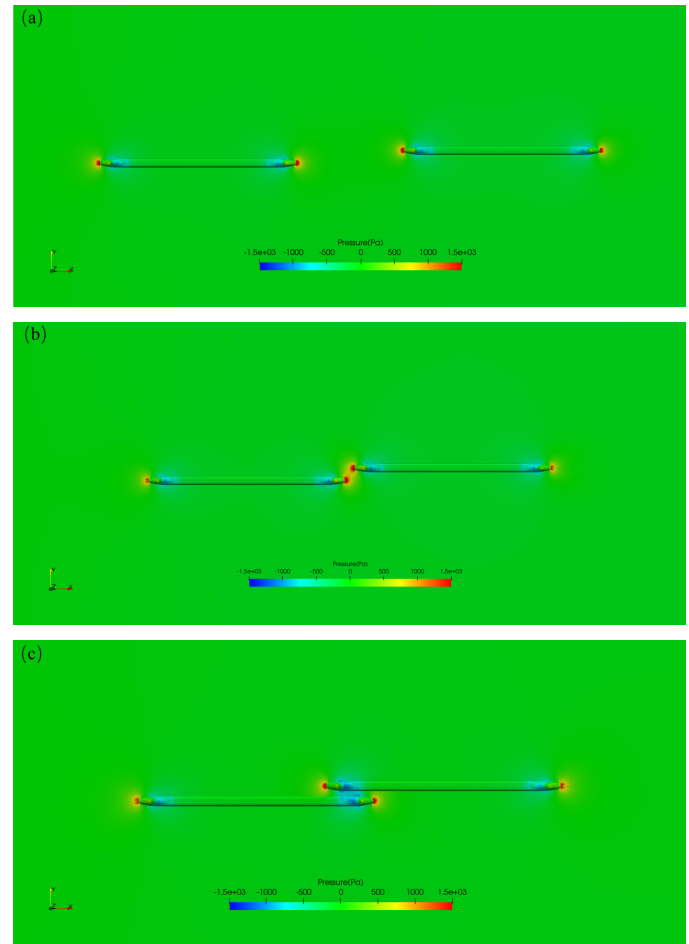


FIGURE 7. Pressure distribution at different time;(a) $t=0.05s$, (b) $t=0.25s$, (c) $t=0.35s$

Taking the head train moving in the positive direction along x -axis to illustrate the changes in drag force over time. Drag force alters lightly between 0.05s and 0.1s. With two trains getting closer, the drag of head train increases gradually, which is reflected in the time range from 0.1s to 0.26s or so. During the process of two trains meeting, its drag first decreases and then increases. The change of drag over time is shown in FIGURE 8. To sum up, the change in drag force over time is basically the same as that in pressure distribution of head train.

Conclusion

In the paper, both cases that flow passing a high-speed train and two trains meeting towards each other in open air are numer-

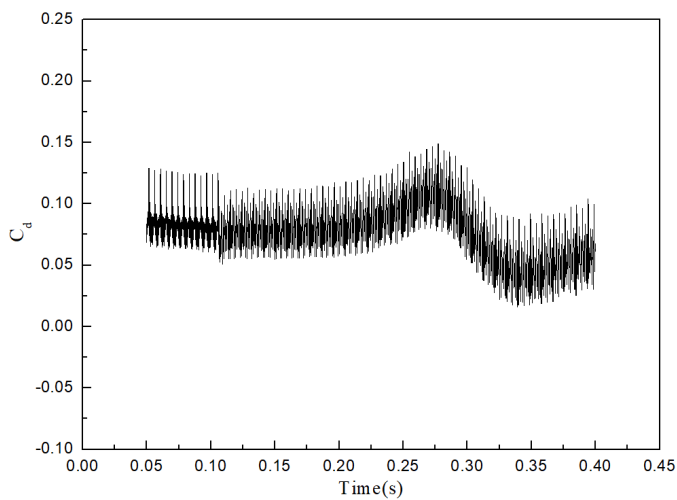


FIGURE 8. Drag coefficient of head train over time

ically simulated. As for the case of flow passing a high-speed train, the aerodynamic results including pressure distribution, velocity distribution and drag coefficient obtained by openFOAM and Star CCM+ are compared. It is found that the pressure distribution by openFOAM and Star CCM+ on the whole train are similar but the drag coefficients are different especially in head train and tail train. Additionally, the simulation of two trains meeting towards each other is conducted to explore the application of overset mesh method, and the change in drag force over time is basically the same as that in pressure distribution of head train.

ACKNOWLEDGMENT

This work is supported by the National Key Research and Development Program of China (2017YFB0202800), the Informatization Plan of the Chinese Academy of Sciences (XXH13506-204) and Strategic Priority Research Program of the Chinese Academy of Sciences (XDB22020101).

REFERENCES

- [1] Baker, C., 1986. "Train aerodynamic forces and moments from moving model experiments". *Journal of Wind Engineering and Industrial Aerodynamics*, **24**(3), pp. 227–251.
- [2] Brockie, N., and Baker, C., 1990. "The aerodynamic drag of high speed trains". *Journal of Wind Engineering and Industrial Aerodynamics*, **34**(3), pp. 273–290.
- [3] Auvity, B., Bellenoue, M., and Kageyama, T., 2001. "Experimental study of the unsteady aerodynamic field outside a tunnel during a train entry". *Experiments in Fluids*, **30**(2), pp. 221–228.
- [4] Matschke, G., and Heine, C., 2002. "Full scale tests on side wind effects on trains. evaluation of aerodynamic coefficients and efficiency of wind breaking devices". In *TRANSAEROA European Initiative on Transient Aerodynamics for Railway System Optimisation*. Springer, pp. 27–38.
- [5] Baker, C., 2002. "The wind tunnel determination of cross-wind forces and moments on a high speed train". In *TRANSAEROA European Initiative on Transient Aerodynamics for Railway System Optimisation*. Springer, pp. 46–60.
- [6] Suzuki, M., Tanemoto, K., and Maeda, T., 2003. "Aerodynamic characteristics of train/vehicles under cross winds". *Journal of wind engineering and industrial aerodynamics*, **91**(1-2), pp. 209–218.
- [7] Sanquer, S., Barre, C., de Virel, M. D., and Cleon, L.-M., 2004. "Effect of cross winds on high-speed trains: development of a new experimental methodology". *Journal of Wind Engineering and Industrial Aerodynamics*, **92**(7-8), pp. 535–545.
- [8] Baker, C., Jones, J., Lopez-Calleja, F., and Munday, J., 2004. "Measurements of the cross wind forces on trains". *Journal of Wind Engineering and Industrial Aerodynamics*, **92**(7-8), pp. 547–563.
- [9] Cheli, F., Ripamonti, F., Rocchi, D., and Tomasini, G., 2010. "Aerodynamic behaviour investigation of the new e-muv250 train to cross wind". *Journal of Wind Engineering and Industrial Aerodynamics*, **98**(4-5), pp. 189–201.
- [10] Wang, H., Zhang, X.-z., Peng, W.-h., and Ma, L.-n., 2011. "Research on aerodynamic characteristics of the high-speed train under side wind". In *International Conference on Computer Science and Information Engineering*, Springer, pp. 401–409.
- [11] Xiang, H., Li, Y., Chen, S., and Li, C., 2017. "A wind tunnel test method on aerodynamic characteristics of moving vehicles under crosswinds". *Journal of Wind Engineering and Industrial Aerodynamics*, **163**, pp. 15–23.
- [12] Yang, G., Guo, D., Yao, S., and Liu, C., 2012. "Aerodynamic design for china new high-speed trains". *Science China Technological Sciences*, **55**(7), pp. 1923–1928.
- [13] Yang, Q.-S., Song, J.-H., and Yang, G.-W., 2016. "A moving model rig with a scale ratio of 1/8 for high speed train aerodynamics". *Journal of Wind Engineering and Industrial Aerodynamics*, **152**, pp. 50–58.
- [14] Ricco, P., Baron, A., and Molteni, P., 2007. "Nature of pressure waves induced by a high-speed train travelling through a tunnel". *Journal of Wind Engineering and Industrial Aerodynamics*, **95**(8), pp. 781–808.
- [15] Li, Z.-w., Yang, M.-z., Huang, S., and Liang, X., 2017. "A new method to measure the aerodynamic drag of high-speed trains passing through tunnels". *Journal of Wind Engineering and Industrial Aerodynamics*, **171**, pp. 110–120.
- [16] Niu, J.-q., Zhou, D., and Liang, X.-f., 2017. "Experimental research on the aerodynamic characteristics of a high-speed train under different turbulence conditions". *Experimental Thermal and Fluid Science*, **80**, pp. 117–125.
- [17] Khier, W., Breuer, M., and Durst, F., 2002. "Numerical computation of 3d turbulent flow around highspeed trains under side wind conditions". In *TRANSAEROA European Initiative on Transient Aerodynamics for Railway System Optimisation*. Springer, pp. 75–86.
- [18] Fauchier, C., Le Devehat, E., and Gregoire, R., 2002. "Numerical study of the turbulent flow around the reduced-scale model of an inter-regio". In *TRANSAEROA European Initiative on Transient Aerodynamics for Railway System Optimisation*. Springer, pp. 46–60.

- Optimisation*. Springer, pp. 61–74.
- [19] Asress, M. B., and Svorcan, J., 2014. “Numerical investigation on the aerodynamic characteristics of high-speed train under turbulent crosswind”. *Journal of Modern Transportation*, **22**(4), pp. 225–234.
- [20] Liu, T.-h., Su, X.-c., Zhang, J., Chen, Z.-w., and Zhou, X.-s., 2016. “Aerodynamic performance analysis of trains on slope topography under crosswinds”. *Journal of Central South University*, **23**(9), pp. 2419–2428.
- [21] Shin, C.-H., and Park, W.-G., 2003. “Numerical study of flow characteristics of the high speed train entering into a tunnel”. *Mechanics Research Communications*, **30**(4), pp. 287–296.
- [22] Zhao, J., and Li, R., 2009. “Numerical analysis for aerodynamics of high-speed trains passing tunnels”. In *The Aerodynamics of Heavy Vehicles II: Trucks, Buses, and Trains*. Springer, pp. 239–239.
- [23] Li, X.-h., Deng, J., Chen, D.-w., Xie, F.-f., and Zheng, Y., 2011. “Unsteady simulation for a high-speed train entering a tunnel”. *Journal of Zhejiang University-SCIENCE A*, **12**(12), pp. 957–963.
- [24] Wang, D., Li, W., Zhao, W., and Han, H., 2012. “Aerodynamic numerical simulation for emu passing each other in tunnel”. In *Proceedings of the 1st International Workshop on High-Speed and Intercity Railways*, Springer, pp. 143–153.
- [25] Krajnović, S., 2009. “Optimization of aerodynamic properties of high-speed trains with cfd and response surface models”. In *The Aerodynamics of Heavy Vehicles II: Trucks, Buses, and Trains*. Springer, pp. 197–211.
- [26] Yao, S., Guo, D., Sun, Z., and Yang, Guowei and Chen, D., 2014. “Optimization design for aerodynamic elements of high speed trains”. *Computers & Fluids*, **95**, pp. 56–73.
- [27] Ding, S.-S., Li, Q., Tian, A.-Q., Du, J., and Liu, J.-L., 2016. “Aerodynamic design on high-speed trains”. *Acta Mechanica Sinica*, **32**(2), pp. 215–232.
- [28] Zhang, J., Li, J.-j., Tian, H.-q., Gao, G.-j., and Sheridan, J., 2016. “Impact of ground and wheel boundary conditions on numerical simulation of the high-speed train aerodynamic performance”. *Journal of Fluids and Structures*, **61**, pp. 249–261.
- [29] Ferziger, J. H., Perić, M., and Street, R. L., 2002. *Computational methods for fluid dynamics*, Vol. 3. Springer.